Journal of
Nanoelectronics and Optoelectronics
Vol. 10, pp. 1–11, 2015
www.aspbs.com/jno

ARTICLE

Organic Semiconductor: Graphene-Oxide/*p*-Si Photodiodes

A. Mekki[1], R. O. Ocaya[2], A. Dere[3], Ahmed A. Al-Ghamdi[3], K. Harrabi[1], and F. Yakuphanoglu[3,4,*]

The device parameters of Al/*p*-Si/PCBM:GO/Au diodes were investigated using direct current–voltage (*I–V*), photocurrent and impedance spectroscopy. The ideality factor of the diode was found to depend significantly on GO content. The calculated barrier heights had low variance over the range of illumination intensities per doping level. Under dark conditions the barrier height averaged 0.767 with a variance of less than 40 parts per million and the ideality factors averaged 10.2 ± 0.4, both parameters taken across all the varying GO contents. The high ideality factors (>9) of the heterostructure organic/inorganic diodes are explained in terms of the low carrier mobilities of the organic interlayer. Capacitance–voltage measurements indicate that the capacitance decreases with increasing frequency, suggesting a continuous distribution of interface states over the surveyed 100 kHz to 1.0 MHz frequency range. The photocurrent results indicate that the photocurrent increases with illumination intensity. The Al/*p*-Si/PCBM:GO/Au diode exhibits a similar photosensitivity with an illumination coefficient of approximately 1.23 ± 0.001 over a wider range of PCBM:GO weight ratios and reverse bias. This suggests that the device photoconductivity is reasonably predictable and particularly suited for photoconductive sensing.

Keywords: Graphene Oxide, Organic Semiconductor, Photodiode.

1. INTRODUCTION

There is currently much theoretical and practical interest in graphene oxide (GO) hybrid structures, particularly those that are used in conjunction with organic compounds as scaffolding structures. The interactions between GO and organic nanocomposites have been studied in detail by various researchers using varied methods in the literature. It has been shown that the interactions do not follow a simple donor–acceptor mode but follows a complicated two-way process. Firstly, there is the transfer of an electron from the graphitic domain to the adsorbed/intercalated interlayer, which in the present investigation is phenyl-C61-butyric acid methyl ester (PCBM). For instance, it has also been shown that the adsorption of cobalt phthalocyanine on functionalized graphene yields a tunable hybrid material that allows sensing because of the intrinsic electrical properties provided by functionalized GO and the nanocomposites.[1] It is then followed by feedback from the Co ions through the ligand-like attaching of oxygen functional groups of GO to the central cobalt ions.[2,3] An improved understanding of the mechanisms of transfer and the impact of low mobility of the organic interlayer may open up applications of the nanocomposites to solid-state sensing and photovoltaic applications.[4] In this paper, we report an investigation on the use of the structural hybrid nanocomposites of PCBM with varying contents of graphene oxide in a *p*-Si heterojunction. The resulting Schottky diodes have the structure Al/GO_x:PCBM/*p*-Si/Au, where (x) is the weight fraction of GO in the hybrid. The device parameters are established through the use of different characterization methods. Through detailed characterizations using standard methods we show that the constructed devices have a clear potential in photosensing applications.

[1]Department of Physics, King Fahd University of Petroleum and Minerals Dhahran, 31261, Saudi Arabia
[2]Department of Physics, University of the Free State, South Africa
[3]Department of Physics, Faculty of Science, Firat University, Elazig 23169, Turkey
[4]Department of Physics, Faculty of Science, King Abdulaziz University, Jeddah 21589, Saudi Arabia
*Author to whom correspondence should be addressed.
Email: fyhan@hotmail.com
Received: xx Xxxx xxxx
Accepted: xx Xxxx xxxx

2. EXPERIMENTAL DETAILS

2.1. Preparation of PCBM and GO Hybrid Films

GO was synthesized by the modified Hummers method.[5] Firstly, 2.0 g of graphite was dissolved in 250 mL H_2SO_4 in ice bath with constant stirring for 2 hrs and then 6.0 g $KMnO_4$ and 1.0 g $NaNO_3$ were added while stirring. It was stirred in a water bath for 20 min. After 20 min, 250 mL of de-ionized water was slowly added, and the temperature of the solution was raised to 98 °C for additional 30 min. The reaction was then stopped by adding de-ionized water (300 mL) and H_2O_2 (40 mL, 35%). The color of the solution transformed to brilliant yellow. The obtained powder was washed, filtered, and dried at 50 °C for 2 days. The phenyl-C61-butyric acid methyl ester (PCBM)[6] was dissolved in dicholoro benzene. The synthesized GO was dispersed in deionized water (1.5 mg/mL) using stirring for 10 min. and then ultrasonicated for 2 h. The nanocomposites of PCBM and GO were prepared using PCBM and GO solutions having different weight ratios of GO (0.1, 0.3 and 0.5). The films of PCBM:GO were coated onto the surface of *p*-Si substrate by drop casting. The films were dried at 150 °C for 3 min. Before deposition of the PCBM:GO composite, the native oxide layer of the silicon substrate was etched by HF and then rinsed in deionized water using an ultrasonic bath for 10–15 min. Finally, the silicon wafer was chemically cleaned according to method based

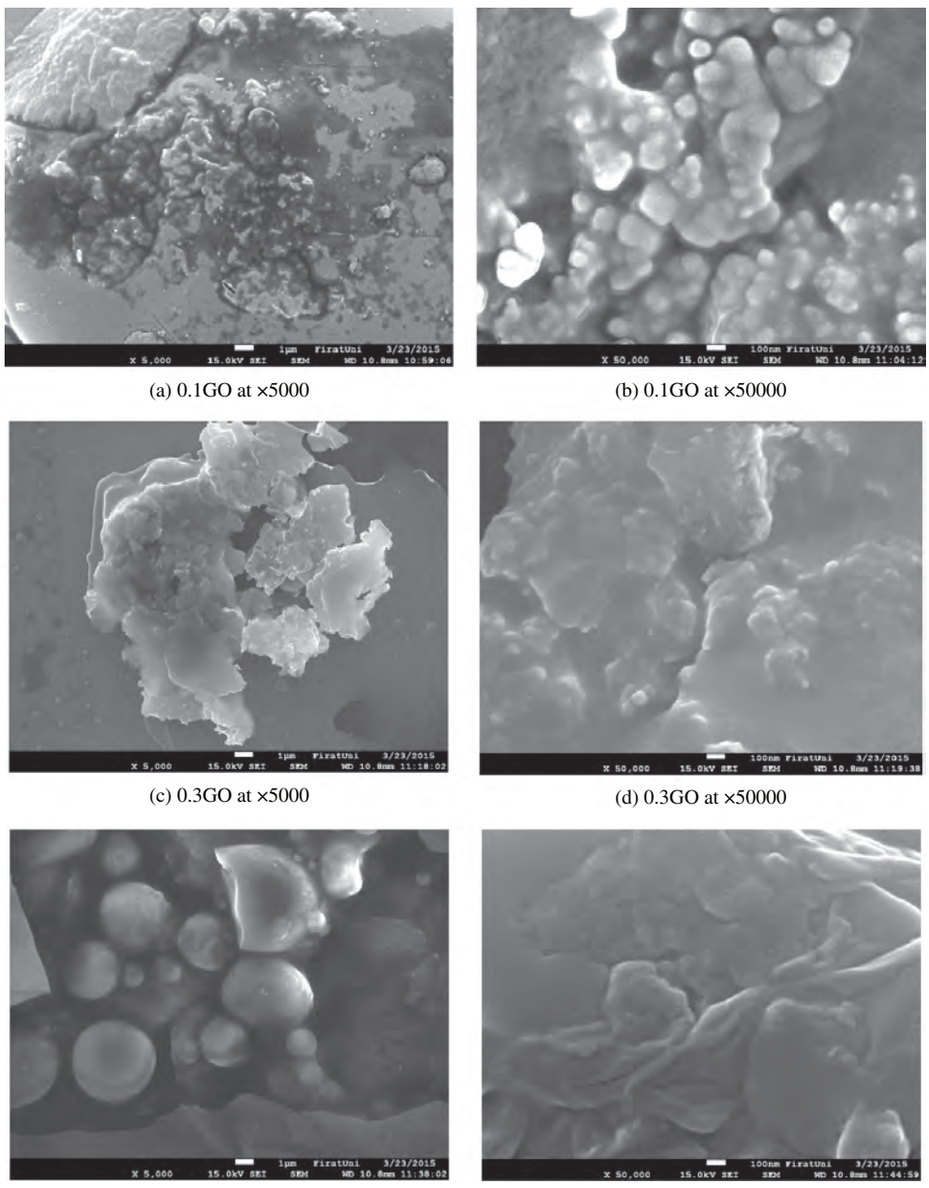

(a) 0.1GO at ×5000 (b) 0.1GO at ×50000

(c) 0.3GO at ×5000 (d) 0.3GO at ×50000

(e) 0.5GO at ×5000 (f) 0.5GO at ×50000

Fig. 1. SEM images at different magnifications of GO:doped PCBM at 0.1, 0.3 and 0.5 weight ratios.

on successive baths of methanol and acetone. The top contact of the diodes was Au metal, obtained by sputtering system in the form of circles with area of 3.14×10^{-2} cm^2. Surface morphology of the films was investigated using a scanning electron microscopy (SEM). The current–voltage (I–V) characteristics of the diode were performed with KEITHLEY 4200 semiconductor characterization system. Photoresponse measurements were performed using a solar simulator. The intensity of the illumination was measured using a solar power meter (TM-206).

2.2. Structural Properties of PCBM:GO Hybrid Films

The structural properties of PCBM:GO hybrid films were investigated by scanning electron microscope (SEM). The SEM images of the films are shown in Figure 1. As seen in SEM images, the films are formed from GO and

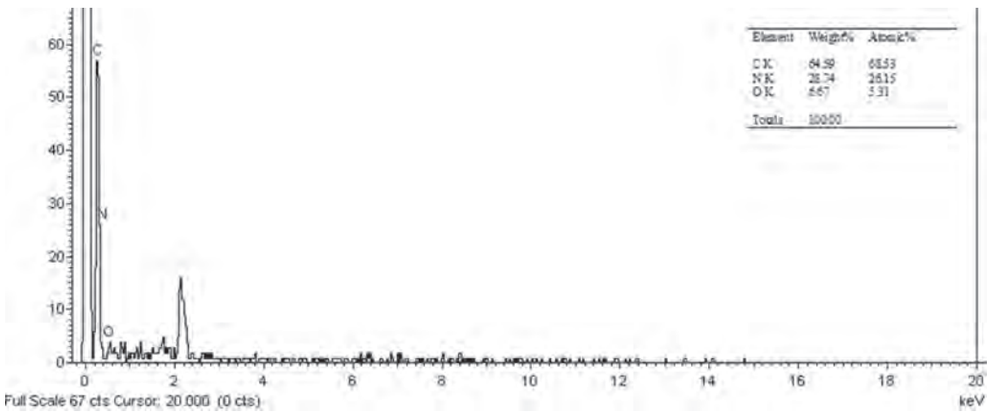

(a) 0.1GO

(b) 0.3GO

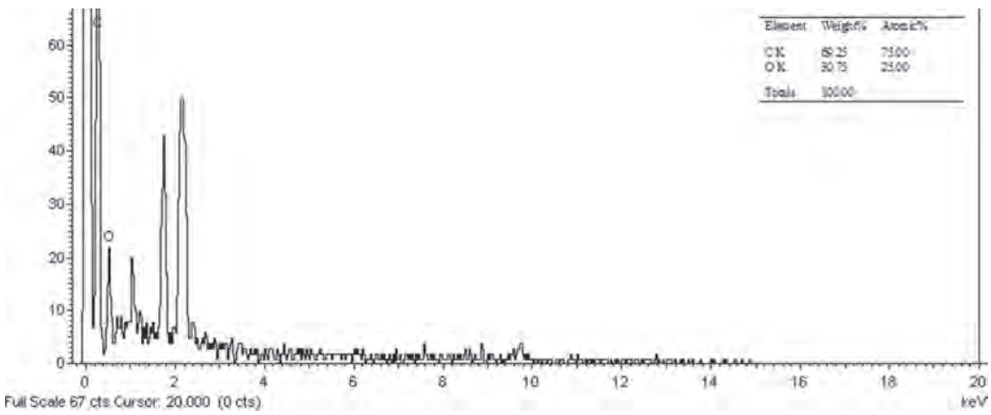

(c) 0.5GO

Fig. 2. EDS spectra of GO:doped PCBM with 0.1, 0.3 and 0.5 weight ratio of PCBM:GO, with insets showing the elemental composition.

PCBM particles. The GO was coated by PCBM particles. The structural properties of the PCBM:GO hybrid films are changed with molar ratio of PCBM:GO organic compound.

Figure 2 shows the EDS spectra of GO:doped PCBM with 0.1, 0.3 and 0.5 weight ratio of PCBM:GO. The embedded insets show the elemental composition of the PCBM:GO. Analysis of the embedded data shows that the percentages of the elements present in the samples are nearly stoichiometric as expected at 0.1, 0.3 and 0.5 GO.

3. RESULTS AND DISCUSSION

The current voltage characteristics (I–V) of the diodes were measured under dark and illumination. Figure 3 shows the I–V characteristics of the diode under different conditions of illumination and GO doping concentration.

Deviations from the ideal thermionic emission theory of the Schottky diode can be explained on the basis of series resistance, popularly estimated using either I–V methods or the method developed by Cheung and Cheung.[7,8] The barrier height (Φ_B), ideality factor (n) and resistance (R_S) are calculated from the following equations:

$$\frac{dV}{d\ln I} = R_s I + n\left(\frac{kT}{q}\right) \tag{1}$$

Over wide ranging currents the plot of $H(I)$ versus I is linear, i.e.,

$$H(I) = R_s I + n\varnothing_B \tag{2}$$

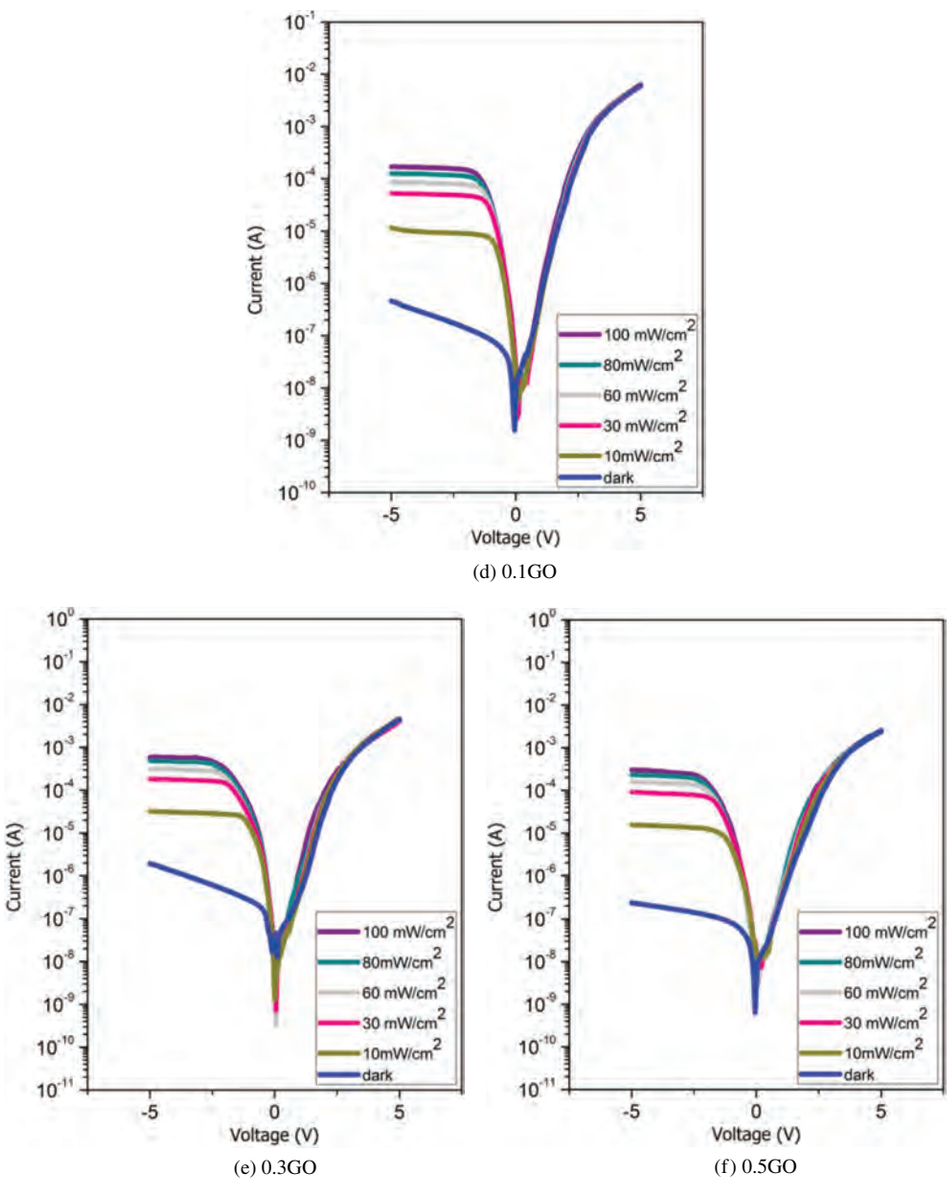

(d) 0.1GO

(e) 0.3GO

(f) 0.5GO

Fig. 3. Current–voltage characteristics of the diode under different illumination intensities and GO doping levels.

where

$$H(I) = V - n\left(\frac{kT}{q}\right)\ln\left(\frac{I}{AA^*T^2}\right) \tag{3}$$

The resistance values obtained using Eqs. (1) and (2) are ideally equal, but the presence of interface states, and a voltage drop across the interfacial layer tends to bring in differences in their values.[9] In the present work it can be seen that they are within the same order of magnitude, and can be said to be equal within analytical bounds.

3.1. Dependence of the *I–V* Characteristics on Illumination Intensity

In Figure 3, which is a plot of the *I–V* characteristics of the Al/*p*-Si/PCBM:GO/Au diode under dark and various illumination intensities and GO concentrations, the typical forward and reverse bias photodiode characteristics are observed. According to thermionic emission theory[10, 11] the current flowing through a rectifying barrier diode as a function of applied bias voltage (V) and temperature (T) is

$$I = I_0 \exp\left[\frac{q(V - IR_s)}{nkT}\right] \tag{4}$$

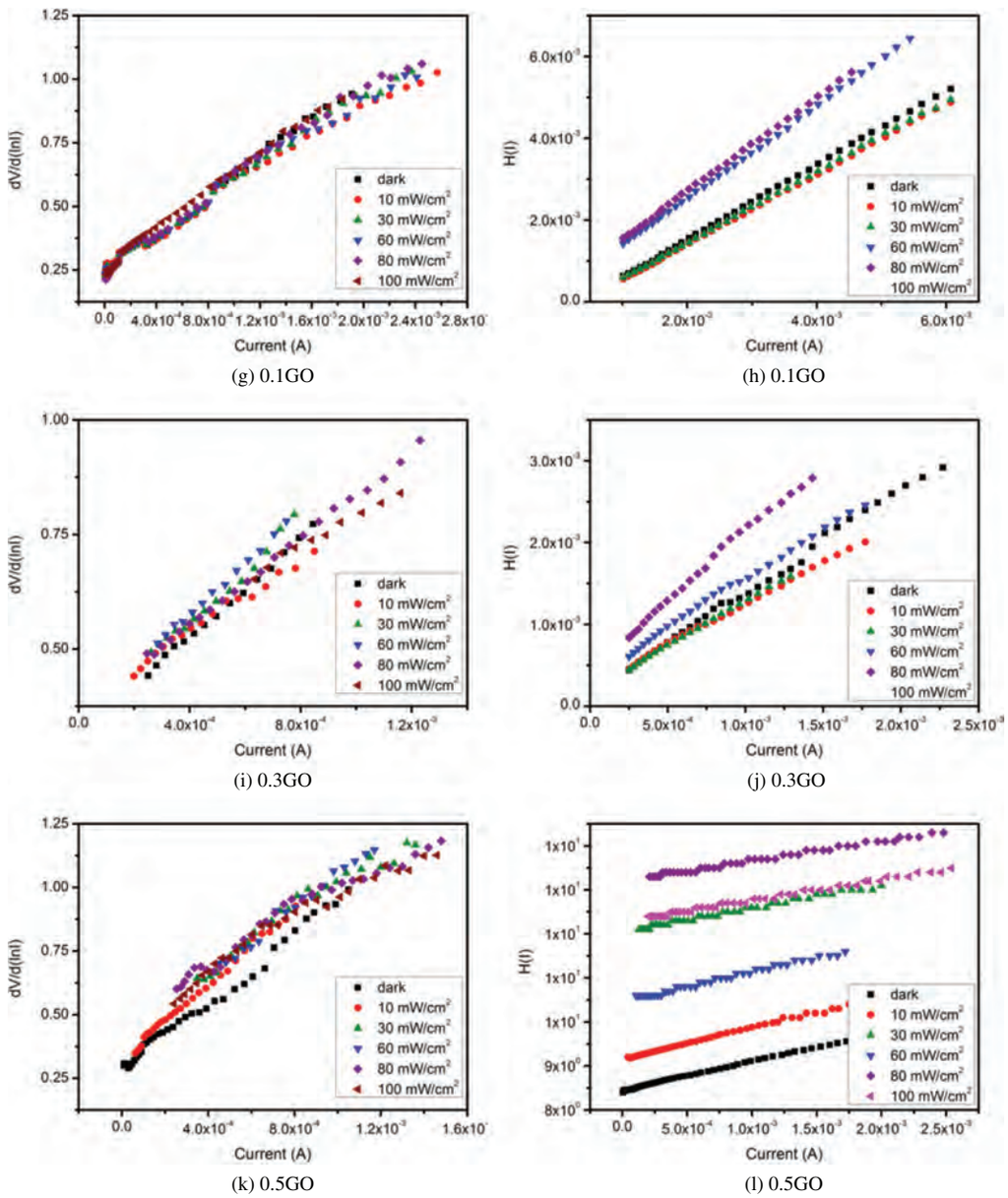

(g) 0.1GO (h) 0.1GO

(i) 0.3GO (j) 0.3GO

(k) 0.5GO (l) 0.5GO

Fig. 4. Current–voltage characteristics obtained using $dV/d(\mathrm{Ln}\,I)$ and $H(I)$ versus current method for different concentrations of GO and illumination intensities.

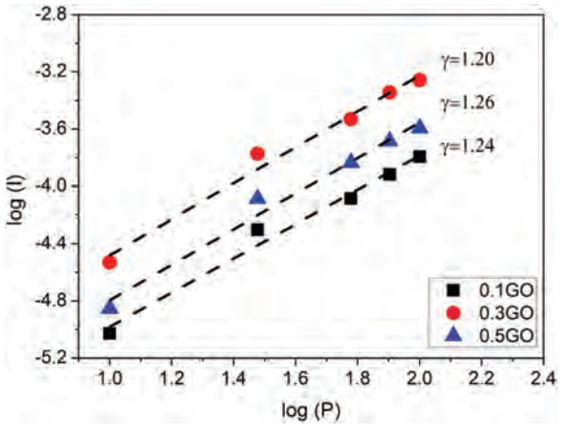

Fig. 5. A plot of the calculated illumination exponents for different GO content at a reverse bias of −3.0 V. The average value of the exponent is $\gamma = \mathbf{1.230 \pm 0.001}$ over the GO content.

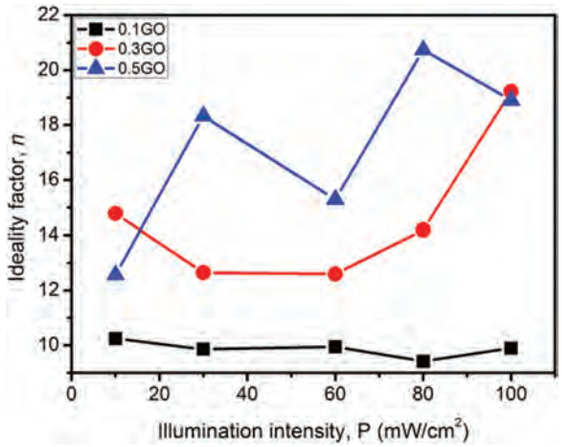

Fig. 6. Variation of calculated ideality factor versus illumination intensity at different concentrations.

where I_0 is the reverse saturation current given by

$$I_0 = AA^*T^2 \exp\left(-\frac{q\varnothing_b}{kT}\right) \tag{5}$$

where q is the electronic charge, A is device area, A^* is the effective Richardson's constant equal to 32A/cm^{2}K^2 for p-Si and $\varnothing_b$ is the barrier height,[12] n is the ideality factor of the diode and k is Boltzmann constant. Barrier height inhomogeneities and the existence of interface states give ideality factors greater than unity.[13] The distribution of interface states can be investigated using photocurrent characterization methods. In Figure 3, an increase in illumination intensity has an associated increase in photocurrent. This suggests that more free carriers are generated upon illumination. For a heterogeneous junction photosensitivity is expressed in terms of the illumination intensity (γ) according to the function

$$I_{PH} = \alpha P^{\gamma} \tag{6}$$

where I_{PH} is the photocurrent, α is a constant.[14, 15] Setting $\alpha = 10^{\beta}$ for a constant β allows Eq. (3) to be rewritten

$$\log I_{PH} = \gamma \log P + \beta \tag{7}$$

which allows γ to be deduced from the log–log plot of diode current versus illumination intensity. Figure 5 is such a plot for the GO doped PCBM interlayer at −3.0 V reverse bias. A higher value of ($\gamma > 0.5$) indicates a lower density of the unoccupied trap level and suggests a less degraded crystal structure and that the recombination mechanism is mononuclear.[13–18] Figure 5 shows a plot of Eq. (7) for concentrations of 0.1GO, 0.3GO and 0.5GO. The calculated coefficient is found to have low variance over the concentration at $\gamma = 1.230 \pm 0.001$, suggesting that in the photoconductive mode the Al/p-Si/PCBM:GO/Al diode can be used over wider doping concentrations for similar photosensitivity. An inspection of the reverse bias region of the I–V plots also suggests that similar sensitivity figures may be obtained at a wider range of bias voltages.

Table I summarizes the parameters of the Al/p-Si/PCBM:GO/Au diodes having varied GO weight fraction over a wide range of illumination intensity. The large ideality factor suggests significant deviations from the thermionic emission theory of the Schottky diode.[10] It has been reported[14] that the barrier height in many heterojunction devices varies with illumination intensity, according to

$$\Phi_b = \Phi_{b0} - \alpha P \tag{8}$$

Table I. Al/p-Si/PCBM:GO/Au diode parameters using the $dV/d(\mathrm{Ln}\, I)$ and $H(I)$ current–voltage methods.

	0.1 GO				0.3 GO				0.5 GO			
	I–V		*H–I*		*I–V*		*H–I*		*I–V*		*H–I*	
Intensity (mW/cm^2)	n	R_s(Ω)		Φ (eV)	n	R_s(Ω)		Φ (eV)	n	R_s(Ω)		Φ (eV)
Dark	9.75	369	310	0.760	10.03	632	416	0.768	10.93	670	655	0.772
10	10.25	313	281	0.751	14.79	393	371	0.675	12.57	743	689	0.729
30	9.86	345	294	0.756	12.65	582	589	0.696	18.33	543	527	0.658
60	9.95	336	289	0.752	12.60	597	570	0.712	15.30	662	650	0.685
80	9.42	370	311	0.759	14.20	472	471	0.680	20.74	448	450	0.637
100	9.90	381	320	0.739	19.23	287	291	0.633	18.91	476	475	0.650

where P is illumination intensity and α is the illumination coefficient ($eV \cdot m^2/W$). The average barrier heights and calculated variance at each illumination with respect to changes in the doping fraction are 0.767 ± 0.000, 0.718 ± 0.002, 0.703 ± 0.002, 0.716 ± 0.001, 0.692 ± 0.004 and 0.674 ± 0.003 eV for the dark, 10 mW/cm^2, 30 mW/cm^2, 60 mW/cm^2, 80 mW/cm^2 and 100 mW/cm^2 illumination intensities respectively. These values suggest that GO concentration does not significantly affect the barrier height. However, the obtained results appear to agree with Eq. (8), with an illumination coefficient of approximately 1.1×10^{-4} $eV \cdot m^2/W$. Soylu et al.[14] have reported an illumination coefficient for a p-Si/$GaFeO_3$ heterostructure Schottky diode of 2.52×10^{-4} $eV \cdot m^2/W$, which is comparable in magnitude to the silicon band gap thermal coefficient of 4.73×10^{-4} eV/K. In Table I the calculated resistance values using the two methods are in close agreement, although it is well known that the two methods often yield very different values. At low illumination intensities both the barrier heights and the ideality factors appear to have low variance across the doping levels. At higher intensities it is apparent that the ideality factor rises, while barrier height decreases. The latter was established in Eq. (8) above. At low GO doping density illumination has less effect on the ideality factor. Figure 6 summarizes these observations. Similar variations in the ideality factor

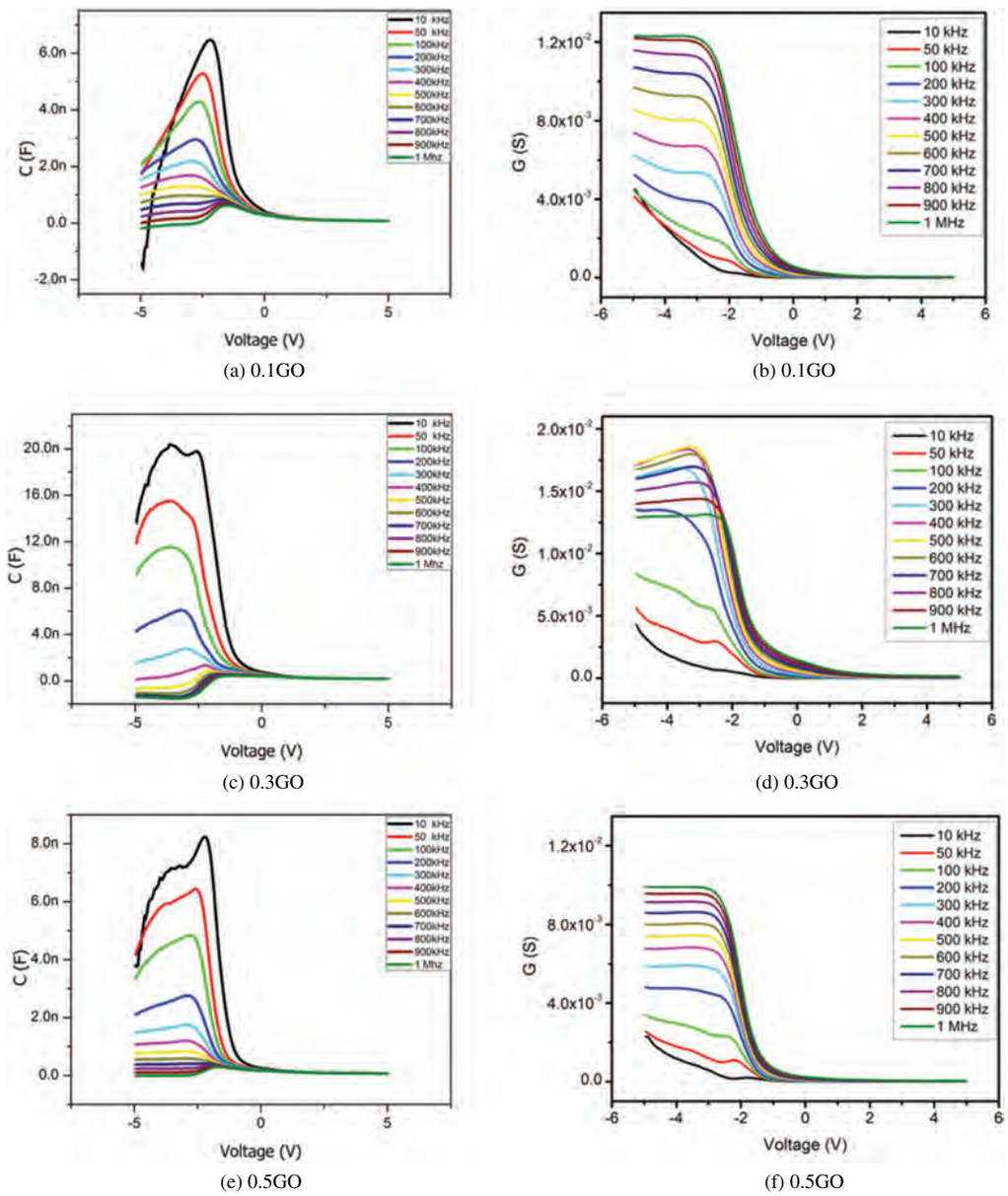

Fig. 7. Capacitance and conductance of the diode versus concentration and different characterization frequencies.

and series resistance were obtained by Würfel et al.[19] under different mobilities. Their work suggests that charge transport on the photovoltaic properties of organic solar cells has a far greater impact that is currently understood. It is typically observed that the analysis of I–V curves of illuminated organic solar cells using the Shockley equation gives ideality factor, photo-current and parallel resistance, which lack physical meaning. This underlying reason for this situation is that drift-diffusion analysis of charge-carrier mobilities versus illumination intensities indicate a pronounced accumulation of charge carriers as a result of poor transport properties. In recent work, the phenomenon has typically been classified together with other effects under the generic term of interface states. Another consequence of this particular that is effectively not modeled in the Shockley equation is that the separation of the quasi Fermi levels in the organic photoactive interlayer, which is expressly the built-in voltage (V_{bi}), differs substantially from the external voltage for almost all conditions of operation. The recent work[19] supports the foregoing assertion of the complexity of the electron transfer mechanisms of the interlayer that is adsorbed or intercalated onto the graphene oxide,[2,3,20] and the need to better understand the interface chemistry.[21,22] They argue that it is meaningless[23,24] to apply the Shockley equation to current–voltage curves under illumination and to extract information on physical parameters such as the recombination order or the apparent Thevenin equivalent resistance R_S in low mobility interlayer semiconductors such as PCBM.[25] There are presently much research effort being spent to understand the impact of the orientational dependence of charge carrier mobilities in organic

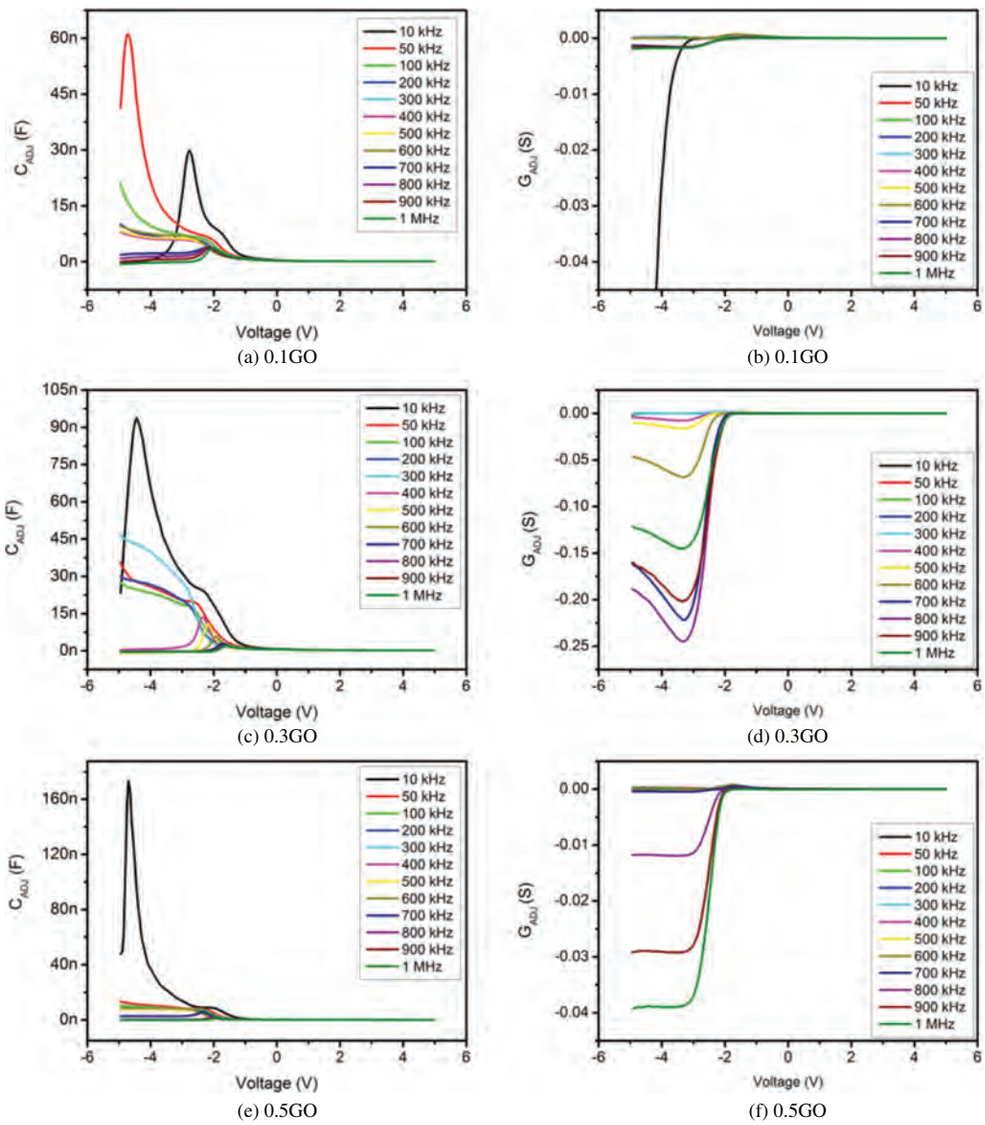

Fig. 8. Calculated adjusted capacitance and conductance of the diode versus concentration and different characterization frequencies.

semiconductor crystals and the correlation with the crystal structure. For instance, Stehr et al.[26, 27] apply quantum chemical first principles calculations combined with a model using hopping rates from Marcus theory in their investigations. The methods used to measure organic semiconductor mobilities are many and give varied values, but some guidelines have been proposed for lowering the variance.[28, 29] In spite of the fact that the consequences of the low electron mobilities are not modeled in Shockley's equation, the implications on ideality factor and resistance are significant in the forward bias of operation. In the present work the primary intent is to use the diode in reverse bias photoconductive mode for photosensing applications and therefore the high forward bias ideality factors and series resistance are not of much concern.

The effects of series resistance and the true-space charge capacitance in the device are taken into account to obtain the corrected capacitance (C_{ADJ}) and conductance (G_{ADJ}) as follows[17, 30–33]

$$C_{ADJ} = \frac{[G_m^2 + (\omega C_m)^2]}{a^2 + (\omega C_m)^2} C_m \tag{9}$$

$$G_{ADJ} = \frac{[G_m^2 + (\omega C_m)^2]}{a^2 + (\omega C_m)^2} a \tag{10}$$

where $a = G_m - [G_m^2 + (\omega C_m)^2]R_s$.

The variation of resistance (R_{S}) with applied bias voltage (V) at different frequencies for different GO content are shown Figure 9. The series resistance of the device is calculated using the equation[12, 14, 34]

$$R_{\mathrm{S}} = \frac{(G_m/\omega C_m)^2}{1 + (G_m/\omega C_m)^2} G_m \tag{11}$$

The $(R_{\mathrm{S}} - V)$ plots exhibit peaks which shift towards higher negative bias voltage as the frequency is increased. The intensity of the peaks decrease with increasing frequency, suggesting that the interface states changes with frequency. At lower frequencies the interface states can follow the AC signal resulting in excess capacitance. At higher frequencies the interface states cannot follow the AC signal and do not make a contribution to interface states.[17, 35, 36]

3.2. Transient Photocurrent Measurements

Figure 10 shows the transient photocurrent measurements of the photodiode as a function of illumination intensity. When the illumination is turned on the photocurrent initially increases rapidly up to a certain level and then gradually reaches a peak value. After the illumination is turned off the photocurrent decreases rapidly at first and then decays to its initial value. The increase in the photocurrent under illumination is due to the increase in the number of free charge carriers increases which contribute to the current. Similarly, after the illumination is turned off the decrease in the photocurrent is due to the trapping

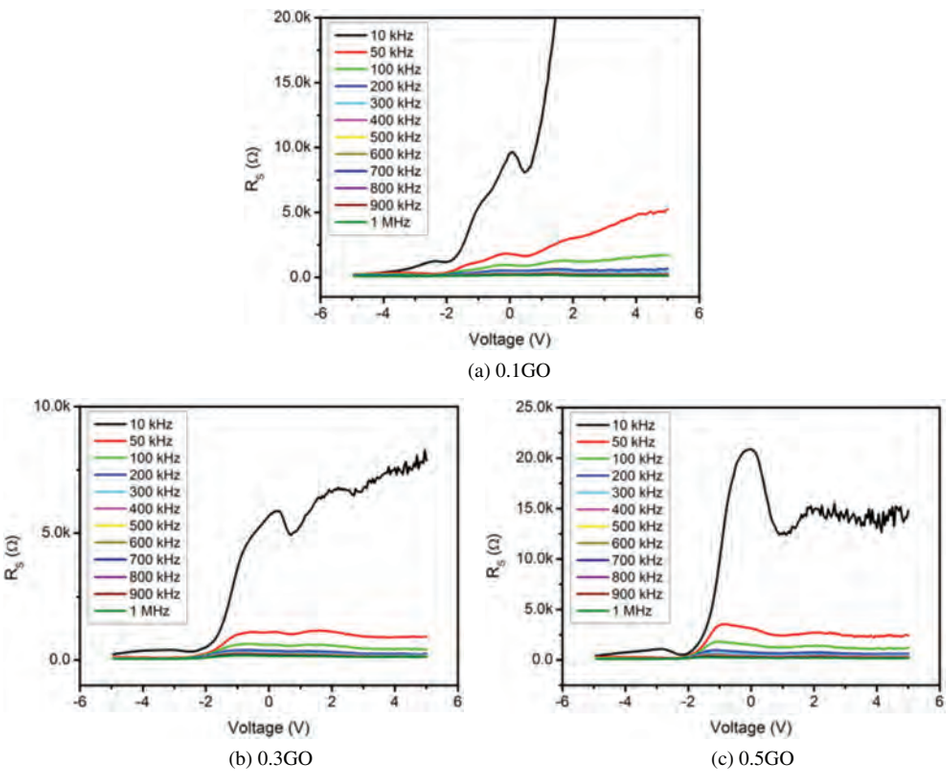

(a) 0.1GO

(b) 0.3GO

(c) 0.5GO

Fig. 9. Variation of series resistance versus voltage at different doping levels.

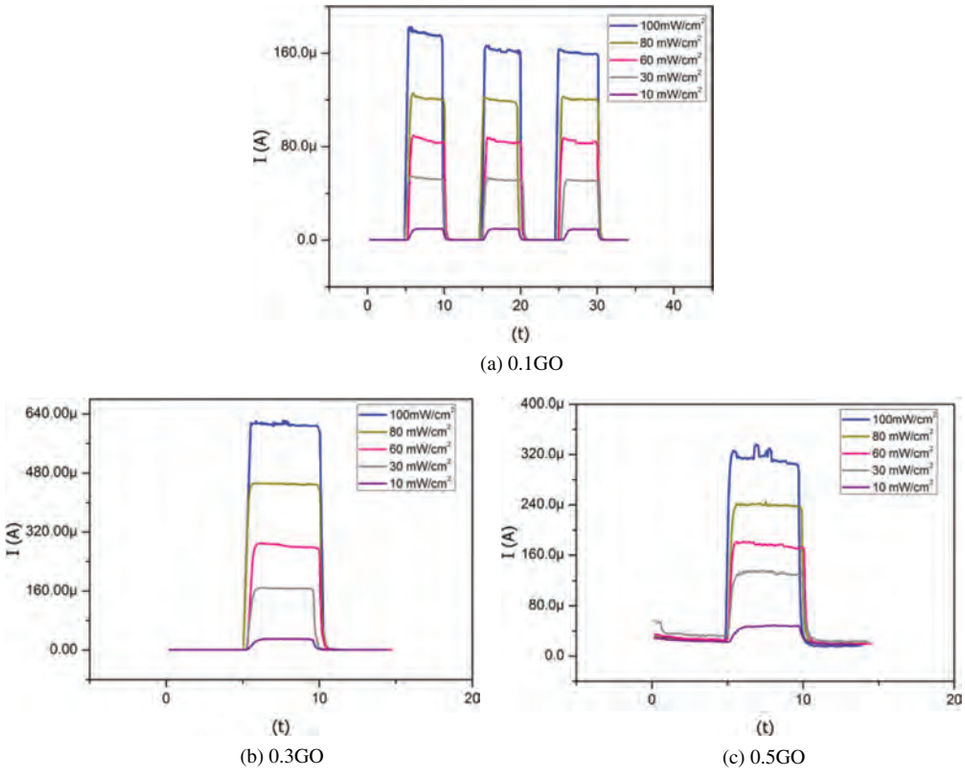

(a) 0.1GO

(b) 0.3GO (c) 0.5GO

Fig. 10. Transient photoresponse of the Al/*p*-Si/PCBM:GO/Al Schottky photodiode at constant reverse bias.

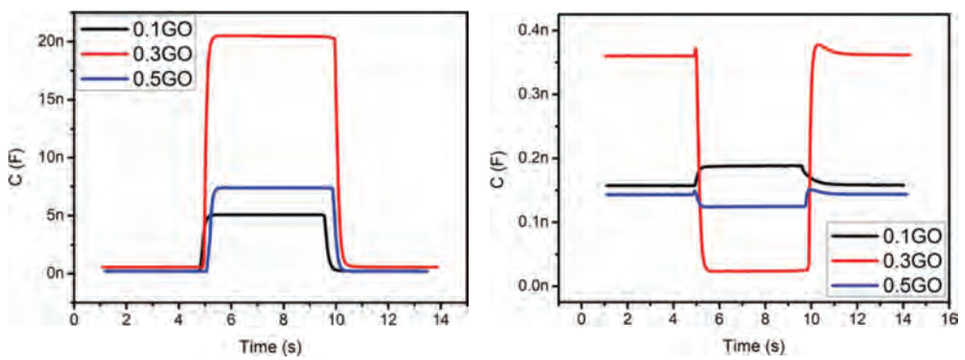

(a) 10 kHz (b) 1 MHz

Fig. 11. Transient photocapacitance taken at 100 mW/cm^2 at 10 kHz and 1 MHz for various PCBM:GO weight ratios.

of the charge carriers in the deep levels, which reduces the current. The device clearly shows photoconducting behavior.

Figure 11 shows the transient photocapacitance of the diodes at 10 kHz and 1 MHz. This data shows that the capacitance of the device depends very strongly on the illumination intensity, the frequency and also the PCBM:GO weight ratio. The highest photocurrent was observed at the 0.3GO PCBM:GO weight ratio at any given incident intensity. At 10 kHz the 0.3GO also exhibited the largest photocapacitance, which became very small at 1 MHz. The device therefore exhibits a photocapacitive behaviour.

4. CONCLUSIONS

In this paper we report on the fabrication and characterization of an organic on inorganic *p*-Si Schottky diode with the structure Al/*p*-Si/PCBM:GO/Au. The device parameters were evaluated using current–voltage, capacitance–voltage and phototransient methods with respect to the fraction of graphene-oxide to phenyl-C61-butyric acid methyl ester (PCBM) ratio. These measurements indicate that the Schottky diode is sensitive to light and there exists the possibility to optmize its performance based on the content of GO. It has been observed in the present analysis that the device photoconductive sensitivity shows

low variance at the investigated PCBM:GO weight ratios and averages approximately 1.23. The highest photoresponse current and the most tunable photocapacitance was observed for a weight ratio of 0.3GO. The calculated ideality factor and series resistance are in agreement with recent studies for low mobility organic semiconductors.

Acknowledgments: Three of the authors (A. Mekki, K. Harrabi and F. Yakuphanoglu) would like to thank The Deanship of Scientific Research at KFUPM for supporting this work under project #IN141009.

References and Notes

1. G. I. Cárdenas-Jirón, P. León-Plata, D. Cortes-Arriagada, and J. M. Seminario, *J. Phys. Chem. C* 117, 23664 **(2013)**.
2. J.-He Yang, Y. Gao, W. Zhang, P. Tang, J. Tan, A.-H. Lu, and D. Ma, *J. Phys. Chem. C* 117, 3785 **(2013)**.
3. B. N. Figgis, E. S. Kucharski, and P. A. Reynolds, *J. Am. Chem. Soc.* 111, 1683 **(1989)**.
4. A. Tataroğlu, H. Tuncer, A. A. Al-Ghamdi, A. Dere, B. Arif, S. Yol, N. Ozdemir, F. El-Tantawy, and F. Yakuphanoğlu, *Synthetic Metals* 206, 15 **(2015)**.
5. W. S. Hummers and R. E. Offeman, *J. Am. Chem. Soc.* 80, 1339 **(1958)**.
6. C. M. Björström, A. Bernasik, J. Rysz, A. Budkowski, S. Nilsson, M. Svensson, M. R. Andersson, K. O. Magnusson, and E. Moons, *J. Phys.: Condens. Matter* 17, L529 **(2005)**.
7. S. K. Cheung and N. W. Cheung, *Appl. Phys. Lett.* 85 **(1986)**.
8. D. T. Phan, R. K. Gupta, G. S. Chung, A. A. Al-Ghamdi, O. A. Al-Hartomy, F. El-Tantawy, and F. Yakuphanoğlu, *Sol. Energy* 86, 2961 **(2012)**.
9. R. K. Gupta, K. Ghosh, and P. K. Kahol, *Physica E* 41, 617 **(2009)**.
10. S. M. Sze, Physics of Semiconductor Device, Second edn., John Wiley & Sons, New York **(1981)**.
11. E. H. Rhoderick and R. H. Williams, Metal-Semiconductor Contacts, Second edn., Clarendon Press, Oxford **(1988)**.
12. R. K. Gupta and R. A. Singh, *Mater. Chem. Phys.* 86, 279 **(2004)**.
13. F. Yakuphanoğlu and B. F. Senkal, *Synth. Met.* 159, 311 **(2009)**.
14. M. Soylu, M. Cavas, A. A. Al-Ghamdi, Z. H. Gafer, F. El-Tantawy, and F. Yakuphanoğlu, *Sol. Energy Mater. Sol. Cells* 124, 180 **(2014)**.
15. S. Kazim, V. Alia, M. Zulfequar, M. M. Haq, and M. Husain, *Physica B* 393, 310 **(2007)**.
16. A. Rose, Concepts in Photoconductivity, Interscience, New York **(1963)**.
17. R. K. Gupta and F. Yakuphanoğlu, *Sol. Energy* 86, 1539 **(2012)**.
18. N. Camaioni, G. Casalbore-Miceli, G. Beggiato, M. Cristani, and C. Summonte, *Thin Solid Films* 366, 211 **(2000)**.
19. U. Würfel, D. Neher, A. Spies, and S. Albrecht, *Nat. Commun.* 6, 6951 **(2015)**.
20. R. T. Tung, *Applied Physics Reviews* 1, 011304 **(2014)**.
21. X. Liu, J. M. Cole, P. G. Waddell, T.-C. Lin, J. Radia, and A. Zeidler, *J. Phys. Chem. A* 116, 727 **(2012)**.
22. Z.-S. Wang, K. Hara, Y. Dan-Oh, C. Kasada, A. Shinpo, S. Suga, H. Arakawa, and H. Sugihara, *J. Phys. Chem. B* 109, 3907 **(2005)**.
23. S. Schiefer, B. Zimmermann, and U. Würfel, *J. Appl. Phys.* 115, 44506 **(2014)**.
24. S. Albrecht, J. R. Tumbleston, S. Janietz, I. Dumsch, S. Allard, U. Scherf, H. Ade, and D. Neher, *J. Phys. Chem. Lett.* 5, 1131 **(2014)**.
25. A. Kokil, K. Yang, and J. Kumar, *J. Polym. Sci. Part B Polym. Phys.* 50, 1130 **(2012)**.
26. V. Stehr, J. Pfister, R. F. Fink, B. Engels, and C. Deibel, *Phys. Rev. B* 82, 155208 **(2011)**.
27. N. Karl, *Synthetic Metals* 133, 649 **(2003)**.
28. J. C. Blakesley, F. A. Castro, W. Kylberg, G. F. A. Dibb, C. Arantes, R. Valaski, M. Cremona, J. S. Kim, and J.-S. Kim, *Organic Electronics* 15, 1263 **(2014)**.
29. S. Tiwari and N. C. Greenham, *Opt. Quant. Electron.* 41, 69 **(2009)**.
30. I. Dokme, S. Altindal, T. Tunc, and I. Uslu, *Microelectron. Reliab.* 50, 39 **(2010)**.
31. I. Dokme, S. Altindal, and I. Uslu, *J. Appl. Polym. Sci.* **(2012)**, DOI 10:1002/app.36327.
32. E. Dobroka and J. Osvald, *Appl. Phys. Lett.* 65, 575 **(1994)**.
33. E. H. Nicollian and A. Goetzberger, *Bell Syst. Technol. J.* 46, 1055 **(1967)**.
34. B. Gunduz, A. A. Al-Ghamdi, A. A. Hendi, Z. H. Gafer, S. El-Gazzar, F. El-Tantawy, and F. Yakuphanoğlu, *Superlattices Microstruct.* 64, 167 **(2013)**.
35. S. Karatas and A. Turut, *Vacuum* 74, 45 **(2004)**.
36. A. Tombak, Y. S. Ocak, S. Asubay, T. Kilicoglu, and F. Ozkahraman, *Mater. Sci. Semicond. Process.* 24, 187 **(2014)**.